

# Chapter 5

## Design and Evaluation of a New Solar Tower-Based Multi-generation System: Part I, Thermal Modeling



Hamed Ghiasirad, Hadi Rostamzadeh, and Sajjad Nasri

### Nomenclature

#### *Symbols*

$C$	Concentration ratio
$h$	Enthalpy ( $\text{kJ} \cdot \text{kg}^{-1}$ ), convection coefficient ( $\text{W}/\text{m}^2\text{K}$ )
$K$	Conductivity ( $\text{W}/\text{m}\cdot\text{K}$ )
$L$	Length of tube (m)
$S$	Supercritical
$T$	Temperature (K), transcritical
$V$	Wind velocity (m/s)
$X$	Salinity ( $\text{g} \cdot \text{kg}^{-1}$ )

#### *Abbreviations*

$F_r$	View factor
HTR	High-temperature recuperator
HU	Heating unit
LTR	Low-temperature recuperator
MC	Main compressor
MFR	Mass flow ratio
PPTD	Pinch point temperature difference (K)
RC	Recompression compressor
STP	Solar tower power

---

H. Ghiasirad (✉) · S. Nasri

Department of Mechanical Engineering, Faculty of Engineering, Sahand University of Technology, Tabriz, Iran

H. Rostamzadeh

Energy and Environment Research Center, Niroo Research Institute (NRI), Shahrak Ghods, Tehran, Iran

© Springer Nature Switzerland AG 2020

F. Jabari et al. (eds.), *Integration of Clean and Sustainable Energy Resources and Storage in Multi-Generation Systems*,

[https://doi.org/10.1007/978-3-030-42420-6\\_5](https://doi.org/10.1007/978-3-030-42420-6_5)

***Greek Letters***

$\delta$	Thickness (m)
$\varepsilon$	Effectiveness, emissivity
$\eta$	Efficiency (%)
$\lambda$	Conductivity (W/m.K)
$\mu$	Viscosity (Pa.s)
$\omega$	Humidity
$\rho$	Reflectivity, density (kg/m <sup>3</sup> )

***Subscripts and Superscripts***

Ape	Aperture
em	Emissive
Dhum	Dehumidifier
fc	Forced convection
Gen	Generator
Hum	Humidifier
H, Hel	Heliostat
Insi	Inner side of receiver
Insu	Insulation
is	Isentropic
ms	Molten salt
nc	Natural convection
ref	Reflection
Sur	Surface
sw	Seawater
TC	Transcritical compressor
W	Wall

**5.1 Introduction**

Galloping consumption of energy around the world has captivated attention of many scholars to design more efficacious energy conversion systems. While many sectors in industry convert the available energy from one form to another more useful form, the conversion of energy in power plants is highly crucial in the developed civilization today. Numerous schemes are devised to further increase power plant efficiency with considering cost aspect of the procedure, where among all using renewable energy has received a well agreement benefit [1, 2].

Among disparate renewable sources, solar energy has widespread applications in high-tech energy conversion systems. Recently, burgeoning growth in development of the concentrating solar power (CSP) technologies have decreased the initial capital costs associated with the installation at wide areas. Among different tools developed to further extend applicability of CSP technologies, thermal, exergy, and cost analysis are highly commendable tools for performance evaluation of the solar

systems. As the major topic of this chapter covers thermal modeling of an innovative solar-based energy systems and the next chapter covers the exergy and exergy-based cost evaluation of the devised system, thermal modeling part of the solar-based systems is spotlighted.

Multi-generation or poly-generation energy conversion systems preeminently refer to the integrated or combined energy systems which produce several useful forms of energy from the same heat source by managing energy losses associated with different sectors of the plant. The term “combined” or “integrated” should be used more carefully in this regard since each has different meaning in energy systems; nonetheless, they may have been used exchangeably in literature. The term “combined energy system” refers to a proper combination of basic energy units in a way to decrease external waste of energy associated with external flow directing into or out of each subunit. The design procedure associated with this arrangement can be fulfilled by applying pinch technology methods or similar concepts in design of a heat exchanger since heat exchangers are the main part of this combination. In this configuration, any mismatching between cold and hot streams may lead to an evenly huge waste thermal heat and hence the meaning of the combination may be lost. Of course, power generation elements such as turbine and power user components such as compressors/pumps can be externally combined by directing a specific generated power of turbine into a compressor which is mainly more meaningful in pure mechanical-driven energy systems such as mechanical compression cooling (MCC) systems. Referring to the second part of the category, the integrated energy systems deal with the internal misarrangements which lead to low energy conversion performance. Special care must be taken in terms of dealing with such integral energy systems since the configuration is real novel, and inspecting the first law of thermodynamics is indeed a matter of concern. The design procedure related to this type of energy systems can be complex in some scenarios, and hence a proper and practical numerical solution should be performed. In this chapter, we have deliberately used both terms in their proper way in order to prevent any vague understanding. Based upon the discussed terms, a new definition can be proposed for multi-generation systems. Broadly speaking, a multi-generation system refers to an integrated or a combined energy system which is composed of at least two subsystems joined to each other internally or externally to produce two or several different useful forms of energy from a unit heat source.

Based upon the above definition, a combined multi-generation system driven by a solar tower power (STP) setup is devised in this chapter to support the arrangement of the main system in terms of energy or thermal modeling as well as exergy and economic. Thermal modeling of the devised multi-generation system is presented in this chapter and its exergy and economic modeling is delivered in the next chapter. Before we proceed further, it is imperious to elaborate on thermal modeling of the solar-based multi-generation systems carried out in recent years.

Yilmaz [3] devised a new multi-generation system for electricity, cooling/heating, hydrogen, and freshwater production using solar energy absorbed via a solar heliostat. The devised system was composed of a Brayton cycle (BC), an organic Rankine cycle (ORC), a Rankine cycle (RC), a flash desalination unit, an absorption cooling/heating unit, and proton exchange membrane (PEM)

electrolyzer. Based upon the thermal modeling presented, the author has reported thermal efficiency of 78.93% with freshwater production of 0.8862 kg/s and with total power capacity of 18,992 kW. They recommended more study should be performed on the solar field from exergy viewpoint.

Yuksel et al. [4] used absorbed heat of a STP plant as a prime mover of a new multi-generation system to produce hydrogen, liquefaction, hot water, freshwater water, cooling, and heating. They reported a thermal performance of 65.1% and concluded that the solar intensity is the most influential parameter in their designed system.

Yilmaz et al. [5] designed a new multi-generation system driven by a STP plant for multiproductions of electricity, cooling, heating, hydrogen, drying products, and liquefaction. They used a gas turbine (GT) cycle as the top cycle operated with the solar energy instead of the conventional combustion firing. They reported thermal performance of 60.14% and pinpointed that the solar intensity and pinch point temperature difference (PPTD) of the heat recovery steam generator (HRSG) have a dominant effect.

Wu et al. [6] designed a new multi-generation system by using a STP plant to supply the required load of the biomass gasification. Despite high thermal efficiency of 44.26%, they found that the intermittency of solar energy can be serious problem in their devised system due to the presence of the chemical energy storage module.

El-Emam and Dincer [7] used heliostat solar system for power generation via a steam turbine, freshwater production via a reverse osmosis (RO) unit, cooling via an absorption chiller cycle (ACC), and hydrogen via water electrolysis. They supplied water production of 90 kg/s and hydrogen generation of 1.25 kg/h for the related users.

In the light of reviewed literature, it is evident that capturing solar energy for electricity, cooling, heating, and freshwater generation is an urgent solution, especially in arid and semiarid regions. Regarding this requirement, several studies have considered this idea and have proposed new multi-generation system to produce such products. The devised multi-generation is composed of a STP plant, a supercritical CO<sub>2</sub> (S-CO<sub>2</sub>) power cycle, a transcritical CO<sub>2</sub> (T-CO<sub>2</sub>) refrigeration cycle, and a humidification-dehumidification (HDH) unit. The current devised multi-generation system has revealed a promising outcome in terms of thermal efficiency which is competitive from different perspectives. It should be noted that using some portion of the generated electricity instead of thermal energy of S-CO<sub>2</sub> refrigeration cycle is another alternative resolution in the combined energy system which is investigated in this chapter. This deliberation prevents further complexity of the multi-generation systems and increases reliability and availability of the setup since the required electricity can be replaced by the network electricity in the case of shutdown. The rest of this chapter is arranged in the following order. In Sect. 5.5.2, a brief description of the layout is presented. In Sect. 5.5.3, all employed thermal mathematical relations and presumptions are displayed. In Sect. 5.4, results are presented and discussed extensively. Finally, some concluding comments are listed in Sect. 5.5.

### 5.2 Setup Description

The overall layout of the devised solar-based multi-generation system is displayed in Fig. 5.1. The setup encompasses from four subsets of a STP plant, a supercritical CO<sub>2</sub> power cycle, a T-CO<sub>2</sub> refrigeration cycle, and a HDH unit. Molten salt is used as circulating refrigerant through the STP plant without considering a thermal storage tank due to the steady characteristics of the problem.

STP plant includes two subcomponents of a heliostat field and a central receiver. Heliostats receive solar irradiances and reflect them into the aperture region of the central receiver at the top of a tower, using a tracking unit for each heliostat. The receiver becomes hotter as the solar rays are concentrated on its center. Molten salt is used as refrigerant flowing through the pipes inside the receiver. The heated molten

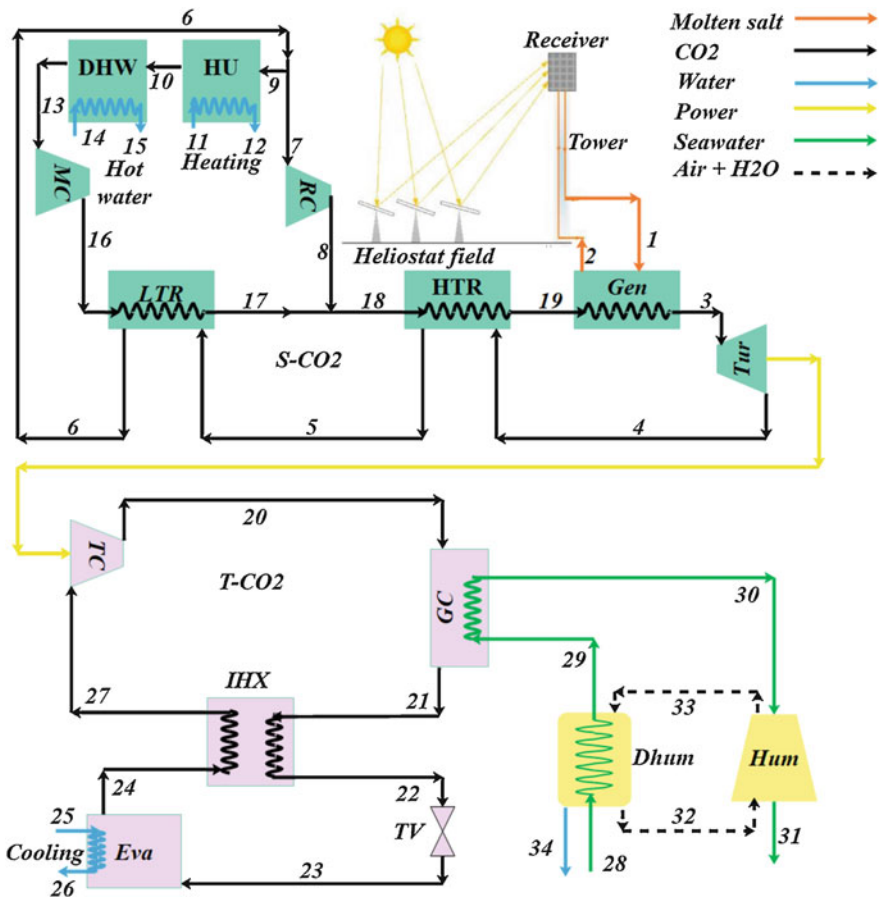


Fig. 5.1 Layout of the devised combined multi-generation system driven by a STP plant

salt is directed to the generator (Gen) and provides required heating load of the S-CO<sub>2</sub> power cycle. Then, the flow is directed back to the receiver.

In S-CO<sub>2</sub> power cycle, the system encompasses a generator, a turbine, a low-temperature recuperator (LTR), a high-temperature recuperator (HTR), a main compressor (MC), an auxiliary compressor or a recompression (RC), a heating unit (HU), and a DHW unit. As the generator receives high-temperature thermal load from the STP plant, the supercritical CO<sub>2</sub> rotates through the turbine to generate electricity and is cooled through two processes by the HTR and LTR to heat the two compressed flows. The cooled stream is split into two flows. One stream flows into the HU to produce the required heating load of the user and then is pre-cooled via a DHW unit prior to the compression process. The flow is compressed through the MC and is heated up through the LTR and is mixed with the rest of the split stream (compressed by RC). The mixed stream is heated up through the HTR and is fed into the generator.

In T-CO<sub>2</sub> refrigeration cycle, a compressor, a gas cooler (GC), an internal heat exchanger (IHX), an evaporator, and a throttling valve (TV) are employed. The supercritical CO<sub>2</sub> is directed to the compressor to boost fluid pressure by consuming some external power supplied by the turbine and then chilled through the gas cooler (GC) at the same pressure. The discarded heating load from the gas cooler is used to provide heating demand of a simple HDH unit. The refrigerant at the outlet of the GC is further cooled via an IHX and then is expanded through a TV. The expanded two-phase stream is vaporized through the evaporator to provide required refrigeration load of the users. The chilled stream is flowed back to the IHX and is directed into the compressor again.

As T-CO<sub>2</sub> refrigeration cycle exchanges its waste heating capacity via a gas cooler with seawater at the HDH side, HDH unit begins its working process. In this study, a basic closed-air open-water (CAOW) HDH unit is used since it has higher efficiency in comparison with its basic closed-water open-air (CWOA) counterpart [8]. As saline water is dehumidified through stage 28→29, it is heated up to the maximum accessible of desalination temperature and is sprayed in a humidifier while leaving it. At the same time, air experiences a successive humidification and dehumidification processes through a closed loop in order to provide evaporation and condensation processes of the seawater. Ultimately, freshwater can be distilled through this integral process via a natural process.

### 5.3 Materials and Methods

Overall, in this section, simulation procedure, presumptions, and relations based on energy/thermal concept are presented. In the first subsection, all relations required for simulation of a STP plant are presented. In the second subsection, thermal presumptions are expressed on the basis of the first law of thermodynamics. Ultimately, the main thermal performance relations are extended.

### 5.3.1 Solar Tower Formulae

Steady mathematical modeling of the solar tower power plant is presented in this section. To better understand the modeling, the structure of the receiver is shown in Fig. 5.2. The receiver absorbs  $\dot{Q}_{\text{rec}}$  from the heliostat field and transfers part of it to the molting salt fluid, while the rest is lost to the ambient by emission, reflection, convection, and conduction, all are expressed as  $\dot{Q}_{\text{rec,totloss}}$  [9].

#### 5.3.1.1 Heliostat

Heliostat field receives solar radiation as [11]:

$$\dot{Q}_{\text{Hel}} = A_h \cdot \text{DNI} \quad (5.1)$$

where  $A_h$  is the total heliostat aperture area and DNI stands for the direct normal irradiation. The total energy that the receiver absorbs from the heliostat is given in terms of the heat absorbed by the receiver ( $\dot{Q}_{\text{rec,abs}}$ ) and total lost heat ( $\dot{Q}_{\text{rec,totloss}}$ ) as [10]:

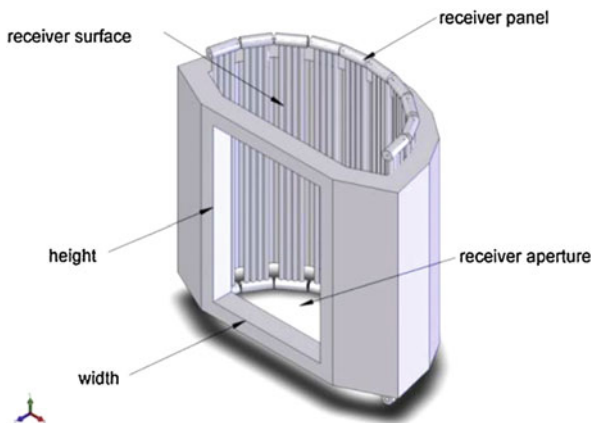
$$\dot{Q}_{\text{rec}} = \dot{Q}_{\text{rec,abs}} + \dot{Q}_{\text{rec,totloss}} \quad (5.2)$$

where

$$\dot{Q}_{\text{rec,abs}} = \dot{m}_{\text{ms}} c_{p,\text{ms}} (T_{\text{ms,out}} - T_{\text{ms,in}}) \quad (5.3)$$

where subscript ms stands for the molten salt. The total heat loss includes emissive (em), reflective (ref), convective (conv), and conductive (con) heat loss as follows [10]:

**Fig. 5.2** Schematic of the receiver [10]



$$\dot{Q}_{\text{rec,totloss}} = \dot{Q}_{\text{rec,em}} + \dot{Q}_{\text{rec,ref}} + \dot{Q}_{\text{rec,conv}} + \dot{Q}_{\text{rec,con}} \quad (5.4)$$

The total energy efficiency of the central receiver can be articulated as:

$$\eta_{\text{rec}} = 1 - \frac{\dot{Q}_{\text{rec,totloss}}}{\dot{Q}_{\text{rec}}} = \frac{\dot{Q}_{\text{rec,abs}}}{\dot{Q}_{\text{rec}}} \quad (5.5)$$

### 5.3.1.2 Receiver Surface Temperature

Before we calculate total losses associated with the receiver, it is imperious to calculate the receiver surface temperature as [10]:

$$T_{\text{rec,sur}} = \frac{\dot{Q}_{\text{rec}}}{\frac{A}{F_r C}} \left[ \frac{d_{\text{out}}}{d_{\text{in}} h_{\text{ms}}} + \frac{d_{\text{out}}}{2k_{\text{tube}}} \ln \frac{d_{\text{out}}}{d_{\text{in}}} \right] + T_{\text{ms}} \quad (5.6)$$

where  $T_{\text{ms}}$  is the characteristic temperature and  $T_{\text{ms}} = (T_{\text{ms, in}} + T_{\text{ms, out}})/2$ .  $d_{\text{in}}$  is the characteristic length.  $h_{\text{ms}}$  is the convective heat transfer coefficient of the molten salt in the absorber tube and is defined as [9]:

$$h_{\text{ms}} = 0.023 \frac{k_{\text{ms}}}{d_{\text{in}}} Re_{\text{ms}}^{0.8} Pr_{\text{ms}}^{0.4} \quad (5.7)$$

where  $k_{\text{ms}}$  is the thermal conductivity of the molten salt and can be found as [11]:

$$k_{\text{ms}} \left[ \frac{W}{m.K} \right] = 0.443 + 1.9 \times 10^{-4} \times T_{\text{ms}} [^{\circ}\text{C}] \quad (5.8)$$

Density, specific heat, and absolute viscosity of the molten salt are also required to obtain Prandtl number (Pr) and Reynolds number (Re), which are calculated, respectively, as follows [9, 11]:

$$\rho_{\text{ms}} \left[ \frac{\text{kg}}{\text{m}^3} \right] = 2090 - 0.636 \times T_{\text{ms}} [^{\circ}\text{C}] \quad (5.9)$$

$$c_{p,\text{ms}} \left[ \frac{\text{J}}{\text{kg.K}} \right] = 1443 + 0.172 \times T_{\text{ms}} [^{\circ}\text{C}] \quad (5.10)$$

$$\mu_{\text{ms}} \left[ \frac{\text{J}}{\text{kg.K}} \right] = (22.714 - 0.12 \times T_{\text{ms}} [^{\circ}\text{C}] + 2.281 \times 10^{-4} \times T_{\text{ms}}^2 [^{\circ}\text{C}] - 1.474 \times 10^{-7} \times T_{\text{ms}}^3 [^{\circ}\text{C}]) \times 10^{-6} \quad (5.11)$$



### 5.3.1.3 Emissive Heat Loss

Only the heat transfer between the aperture and receiver surface is accounted as follows [11]:

$$\dot{Q}_{\text{rec,em}} = \frac{\epsilon_{\text{avg}} \sigma (T_{\text{rec,sur}}^4 - T_{\text{air}}^4) A_{\text{field}}}{C} \quad (5.12)$$

where  $C$  is the concentration ratio and  $\sigma = 5.67 \times 10^{-8} \text{ W} \cdot \text{m}^{-2} \cdot \text{K}^{-4}$  is the Stefan-Boltzmann constant.  $\epsilon_{\text{avg}}$  and  $F_r$  are the average emissivity and view factor given, respectively, by [9]:

$$\epsilon_{\text{avg}} = \frac{\epsilon_w}{\epsilon_w + (1 - \epsilon_w) F_r} \quad (5.13)$$

$$F_r = \frac{A_{\text{ape}}}{A_{\text{field}}} \quad (5.14)$$

In Eq. (5.14),  $A_{\text{ape}}$  is the aperture area.

### 5.3.1.4 Reflective Heat Loss

Reflective heat loss due to the surface reflectivity and view factor without considering the receiver surface reflectivity with the receiver surface temperature can be expressed as [10]:

$$\dot{Q}_{\text{rec,ref}} = \dot{Q}_{\text{rec}} \cdot F_r \cdot \rho \quad (5.15)$$

where  $\rho$  is the surface reflectivity.

### 5.3.1.5 Convective Heat Loss

Convective heat loss includes both forced and natural convection heat transfer as [9, 10]:

$$\dot{Q}_{\text{rec,conv}} = \dot{Q}_{\text{rec,conv,fc}} + \dot{Q}_{\text{rec,conv,nc}} \quad (5.16)$$

where

$$\dot{Q}_{\text{rec,conv,fc}} = h_{\text{air,fc,insi}} (T_{\text{rec,sur}} - T_0) \frac{A_{\text{field}}}{C} \quad (5.17)$$

$$\dot{Q}_{\text{rec,conv,nc}} = h_{\text{air,nc,insi}}(T_{\text{rec,sur}} - T_0) \frac{A_{\text{field}}}{F_r C} \quad (5.18)$$

$$h_{\text{air,fc,insi}} = 0.0287 \frac{k_{\text{air}}}{L} Re_{\text{air,insi}}^{0.8} Pr_{\text{air,insi}}^{1/3} \quad (5.19)$$

$$h_{\text{air,nc,insi}} = 0.81 \times (T_{\text{rec,sur}} - T_0)^{0.426} \quad (5.20)$$

In Eq. (5.19),  $L$  is the characteristic length and  $h_{\text{air, fc, insi}}$  and  $h_{\text{air, nc, insi}}$  are the forced and natural convective heat transfer coefficients, respectively.

### 5.3.1.6 Conductive Heat Loss

Only conductive heat loss associated with the insulation layer is accounted as follows:

$$\dot{Q}_{\text{rec,con}} = (T_{\text{insu,w}} - T_0) \frac{A_{\text{field}} h_{\text{air,out}}}{F_r C} \quad (5.21)$$

where ( $n = 1$ ) [10]:

$$h_{\text{air,out}} = (h_{\text{air,nc,out}}^n + h_{\text{air,fc,out}}^n)^{1/n} \quad (5.22)$$

$$h_{\text{air,nc,out}}^n = 1.24 \times (T_{\text{insu,w}} - T_0)^{1/3} \quad (5.23)$$

$$h_{\text{air,fc,out}} = 0.0239 \frac{k_{\text{air}}}{L} Re_{\text{air,out}}^{0.805} \times \left( 0.785 \times \frac{T_{\text{insu,w}}}{T_0} \right)^{0.2} \times 1.167 \times Pr_{\text{air,out}}^{0.45} \quad (5.24)$$

For the calculation of outlet air specifications, consider  $T_{\text{air, out}} = T_0$  [10].  $T_{\text{insu, w}}$  could be fined from Eq. (5.25) [9]:

$$(T_{\text{insu,w}} - T_0) h_{\text{air,out}} = \frac{\lambda_{\text{insu}}}{\delta_{\text{insu}}} (T_{\text{Rec,Sur}} - T_{\text{insu,w}}) \quad (5.25)$$

### 5.3.2 Thermal Presumptions and Evaluation

Subsequent presumptions are made through the analysis:

- Steady-state condition is governed.
- Compressors and turbine operate with an isentropic efficiency.
- Isenthalpic condition prior and after the expansion valve is assumed.

- Temperature of the distilled water is presumed as the average of the exit air dry-bulb temperature and the inlet air dew-point temperature in the dehumidifier [8, 12, 13].
- The exiting and entering air relative humidity is set at 90% [8].
- Around 11.6% of turbine output power is supplied to the compressor of T-CO<sub>2</sub> refrigeration cycle to achieve around 200 kW cooling load [14].
- Pressure drops in HTR, LTR, generator, DHW, and HU are deliberated 3%, 2%, 2%, 1%, and 1%, respectively [15].
- Evaporator outlet is assumed as saturated vapor.
- Water entering the HU, DHW, and evaporator, and the seawater entering the dehumidifier are at ambient pressure and temperature.
- HTR, LTR, humidifier, and dehumidifier work with specific effectiveness of 86% [15].
- Molten salt pressure is equal to ambient pressure [16].
- Molten salt weight percent is 60% NaNO<sub>3</sub> and 40% KNO<sub>3</sub> [16].

Additionally, some other presumptions in terms of input data are listed in Table 5.1.

In terms of mass and energy conservation relations, thermal analysis of a setup may be articulated as:

- Mass balance equation:

$$\sum \dot{m}_{in} - \sum \dot{m}_{out} = 0 \quad (5.26)$$

- Energy balance equation:

$$\dot{Q}_{c.v.} - \dot{W}_{c.v.} = \sum (\dot{m}h)_{out} - \sum (\dot{m}h)_{in} \quad (5.27)$$

Based upon the above-defined relations, the energy balance equations for different constituents of the suggested setup are presented in Table 5.2.

### 5.3.3 Main Thermal Criteria

The first law of thermodynamics for the devised unit is expressed as follows:

$$\eta_{en} = \frac{\dot{W}_{net} + \dot{Q}_{HU} + \dot{Q}_{DHW} + \dot{Q}_{eva} + \dot{m}_{34} \cdot h_{fg@T_{34}}}{\dot{Q}_{Hel}} \quad (5.28)$$

where  $\dot{W}_{net}$ ,  $\dot{Q}_{HU}$ ,  $\dot{Q}_{DHW}$ , and  $\dot{Q}_{eva}$  are the produced net electricity, heating load, DHW heat transfer rate, and refrigeration load, respectively. The net electricity can be expressed as:

**Table 5.1** Input data of poly-generation system

Parameter	Value	Ref.
Ambient temperature, $T_0$ (K)	298.15	[17]
Ambient pressure, $P_0$ (bar)	1	[17]
Direct normal irradiance, DNI ( $\text{kW/m}^2$ )	0.8	[11]
Heliostat area, $A_h$ ( $\text{m}^2$ )	10,000	[11]
Heliostat efficiency, $\eta_h$	0.75	[11]
Sun temperature, $T_{\text{sun}}$ (K)	4500	[11]
Molten salt high temperature, $T_1$ (K)	838.15	[11]
Generator PPTD, (K)	10	—
Tube diameter, $d_i$ (m)	0.019	[11]
Tube thickness, ( $d_o - d_i$ ) (m)	0.00165	[11]
Tube conductivity, $\lambda_{\text{tube}}$ (W/m. K)	23.9	[10]
Emissivity, $\epsilon$	0.8	[11]
Concentration ratio, $C$	1200	[18]
Aperture area of receiver, $A_{\text{ape}}$ ( $\text{m}^2$ )	12.5	[11]
View factor, $F_r$	0.8	[11]
Reflectivity, $\rho$	0.04	[11]
Wind velocity, $V$ (m/s)	5	[11]
High of receiver, $L$ (m)	6	[10]
Insulation layer thickness, $\delta_{\text{insu}}$ (m)	0.07	[10]
Insulation conductivity, $\lambda_{\text{insu}}$ (m)	40	[9]
MC and RC pressure ratio, $PR_{\text{MC, RC}}$	3	[15]
Maximum temperature of S-CO <sub>2</sub> , $T_3$ (K)	823.15	[15]
Turbine isentropic efficiency, $\eta_{\text{is, Tur}}$	0.9	[15]
MC and RC isentropic efficiencies, $\eta_{\text{is, MC, RC}}$	0.85	[15]
Heating unit PPTD, (K)	30	—
Domestic hot water unit PPTD, (K)	15	—
Turbine outlet pressure, $P_4$ (bar)	74	[15]
Mass flow ratio of S-CO <sub>2</sub> , $\dot{m}_7/\dot{m}_6$	0.25	[15]
HU outlet water temperature, $T_{12}$ (K)	353.15	[19]
DHW outlet water temperature, $T_{15}$ (K)	323.15	[20]
Evaporator temperature, $T_{24}$ (K)	273	[21]
Internal heat exchanger PPTD, (K)	5	—
Maximum pressure of T-CO <sub>2</sub> , $P_{20}$ (bar)	90	[21]
T-CO <sub>2</sub> compressor isentropic efficiencies, $\eta_{\text{is, TC}}$	0.7	[21]
Evaporator temperature difference, (K)	10	[21]
Gas cooler PPTD, (K)	25	—
Mass flow ratio of HDH, $\dot{m}_{28}/\dot{m}_{32}$	2.5	[22]
Desalination top temperature, $T_{30}$ (K)	353.15	[22]
Seawater salinity, $X_{28}$ (g/kg)	35	[22]

**Table 5.2** Required energy balances for system analysis

Constituent	Mass and energy balance equations
Heliostat field	$\dot{Q}_{\text{Loss,Hel}} = \dot{Q}_{\text{Hel}} - \dot{Q}_{\text{Rec}}$
Cavity receiver	$\dot{Q}_{\text{Rec}} = \eta_h \dot{Q}_{\text{Hel}}$ $T_2 = T_{19} + \text{PPTD}_{\text{Gen}}$ $T_{\text{Air}} = (T_0 + T_{\text{Rec, Sur}})/2$
Generator	$\dot{m}_{19}(h_{19} - h_{18}) = \dot{m}_4(h_4 - h_5)$
HTR	$e = \frac{T_4 - T_5}{T_4 - T_{18}}$ $P_{17} = P_{18} = P_8$ $\dot{m}_{17}h_{17} + \dot{m}_8h_8 = \dot{m}_{18}h_{18}$
LTR	$e = \frac{T_5 - T_6}{T_5 - T_{16}}$ $\dot{m}_5(h_5 - h_6) = \dot{m}_{17}(h_{17} - h_{16})$
Heating unit	$\dot{m}_{12}(h_{12} - h_{11}) = \dot{m}_9(h_9 - h_{10})$ $T_{10} = T_{11} + \text{PPTD}_{\text{HU}}$
DHW	$\dot{m}_{15}(h_{15} - h_{14}) = \dot{m}_{10}(h_{10} - h_{13})$ $T_{13} = T_{14} + \text{PPTD}_{\text{DHW}}$
T-CO <sub>2</sub> compressor	$\dot{W}_{\text{TC}} = \dot{m}_{20}(h_{20} - h_{27})$ $\text{ER} = \dot{W}_{\text{TC}}/\dot{W}_{\text{Tur}}$
IHX	$T_{27} = T_{21} - \text{PPTD}_{\text{IHx}}$ $h_{21} - h_{22} = h_{27} - h_{24}$
Evaporator	$T_{26} = T_{25} - \text{TD}_{\text{Eva}}$
Hum	$\dot{m}_{28}X_{28} = \dot{m}_{31}X_{31}$ $\dot{m}_{33}(h_{33} - h_{32}) = \dot{m}_{30}h_{30} - \dot{m}_{31}h_{31}$ $\dot{m}_{31} = \dot{m}_{28} - \dot{m}_{34}$ $e = \max\left(\frac{h_{33} - h_{32}}{h_{33,\text{ideal}} - h_{32}}, \frac{h_{30} - h_{31}}{h_{30} - h_{31,\text{ideal}}}\right)$ $h_{33,\text{ideal}} @ T_{30} \ \& \ h_{31,\text{ideal}} @ T_{32}$
Dhum	$\dot{m}_{33}(h_{33} - h_{32}) = \dot{m}_{29}(h_{29} - h_{28}) + \dot{m}_{34}h_{34}$ $\dot{m}_{34} = \dot{m}_{32}(\omega_{33} - \omega_{32})$ $e = \max\left(\frac{h_{29} - h_{28}}{h_{29,\text{ideal}} - h_{28}}, \frac{h_{33} - h_{32}}{h_{33} - h_{32,\text{ideal}}}\right)$ $h_{32,\text{ideal}} @ T_{28} \ \& \ h_{29,\text{ideal}} @ T_{33}$

$$\dot{W}_{\text{net}} = \dot{W}_{\text{tur}} - \dot{W}_{\text{MC}} - \dot{W}_{\text{RC}} - \dot{W}_{\text{TC}} \quad (5.29)$$

## 5.4 Results and Discussion

Table 5.3 exhibits the results of thermal modeling of the devised multi-generation system in terms of chief performance criteria. According to Table 5.3, the devised configuration can produce net electricity of 1335 kW, desalinated water of 34.79 m<sup>3</sup>/day, refrigeration load of 200 kW, heating load of 2870 kW, and hot water of 633 kW. Under such design circumstance, energy efficiency is calculated 74.81% which can further be increased by manipulating some input data which is discussed in parametric study section.

**Table 5.3** Important thermal modeling analysis of multi-generation system

Parameter	Value
Receiver energy efficiency (%)	87.91
Heliostat heat input (kW)	8000
Receiver input energy (kW)	6000
Receiver total energy loss (kW)	725.2
DHW heating load (kW)	633
HU heating load (kW)	2870
Turbine power output	3766
MC power consumption (kW)	1207
RC power consumption (kW)	787.9
Refrigeration load (kW)	200
COP of T-CO <sub>2</sub> refrigeration	0.4589
TC power consumption (kW)	436.9
Freshwater production (m <sup>3</sup> /day)	34.79
Gained output ratio (GOR) of HDH	1.484
Net power output (kW)	1335
Energy efficiency (%)	74.81

## 5.5 Parametric Study

In this section, the most important parameters were studied in order to obtain their impacts on energy efficiency.

### 5.5.1 Effect of Direct Normal Irradiance

The first effect of direct normal irradiance (DNI) can be seen in Fig. 5.3, in which with increasing DNI, energy efficiency decreases. The decrease of thermal efficiency with increasing DNI is because of high increase in solar heat transfer rate. Although net power output, heating and DHW values have a small increase and cooling and desalination values are constant, solar energy input has a big increment and for this reason efficiency will be decreased. So, it is suitable selection to have a minimum DNI to maximize the first law efficiency.

### 5.5.2 Effect of Receiver Concentration Ratio

Receiver concentration ratio is an important parameter because it affects the receiver surface temperature, conduction, convection, and radiation heat losses. Its effect can be seen in Fig. 5.4 that its increase causes higher energy efficiency. With increasing receiver concentration ratio, the receiver surface temperature and aperture area will be increased and decreased, respectively. Increasing the receiver temperature causes

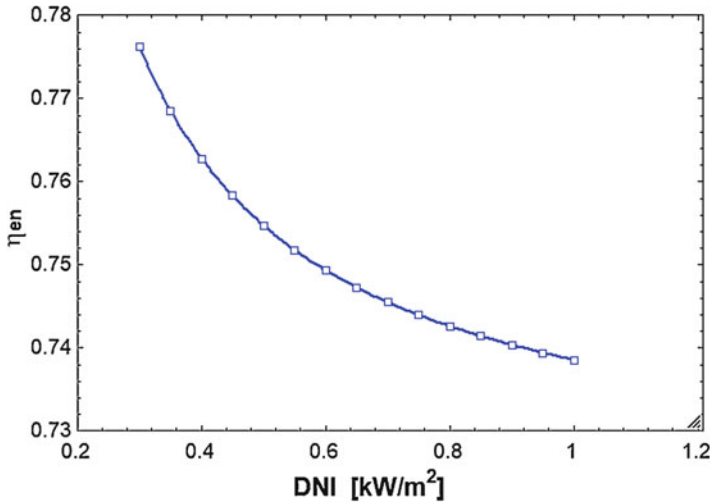


**Fig. 5.3** Effect of DNI on thermal efficiency of the system

small increase of heat losses, but decreasing the aperture area causes high decrease of heat losses. So, the overall decrease of heat losses is good reason of increasing the first law efficiency and it is good selection for concentration ratio to be as high as possible for obtaining higher energy efficiency (Fig. 5.4).

### 5.5.3 *Effect of Generator Pinch Point Temperature Difference*

Considering Fig. 5.5, with increasing generator pinch point temperature difference, energy efficiency will be decreased. The reason of this effect is the decreasing net power, heating, and DHW values, while cooling, desalination, and solar energies are constant.

### 5.5.4 *Effect of MC and RC Pressure Ratio*

Considering Fig. 5.6, there is an increase in energy efficiency with increasing pressure ratio. With this increment, cooling, desalination, and solar heat transfer rates are constant, but the net power and DHW values have decreased and heating heat transfer rate has a higher increase. So, the heating energy increase causes an increase in thermal efficiency. So, in higher pressure ratios, energy efficiency will be higher.

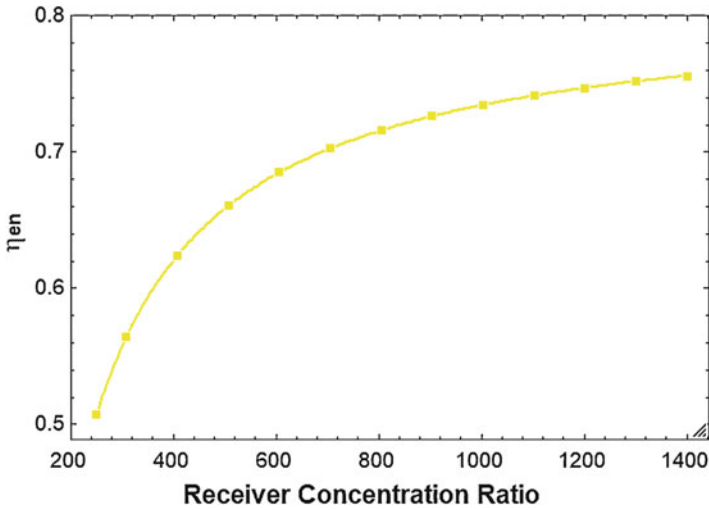


Fig. 5.4 Effect of receiver concentration ratio on thermal efficiency of the system

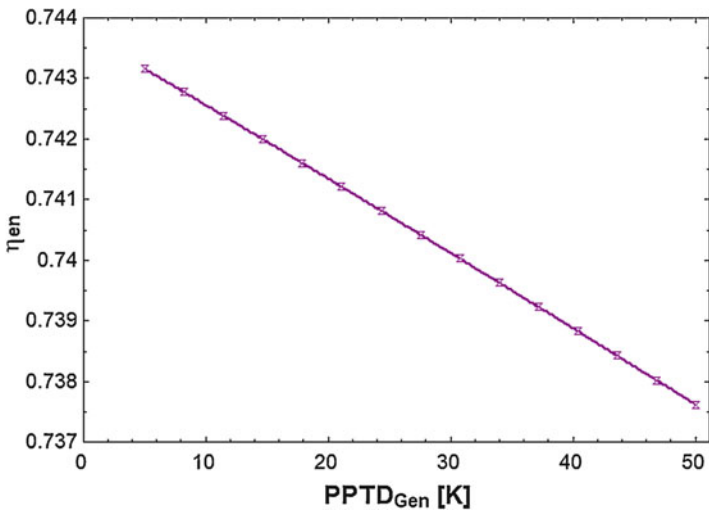


Fig. 5.5 Effect of generator PPTD on thermal efficiency of the system

### 5.5.5 Effect of HTR, LTR, Hum, and Dhum Effectiveness

Effectiveness is one of the main parameters that has high effect on objectives because it has the same value for HTR, LTR, Hum, and Dhum. It is clear that high effectiveness values result to high performance of heat exchangers and better energy efficiency (Fig. 5.7).



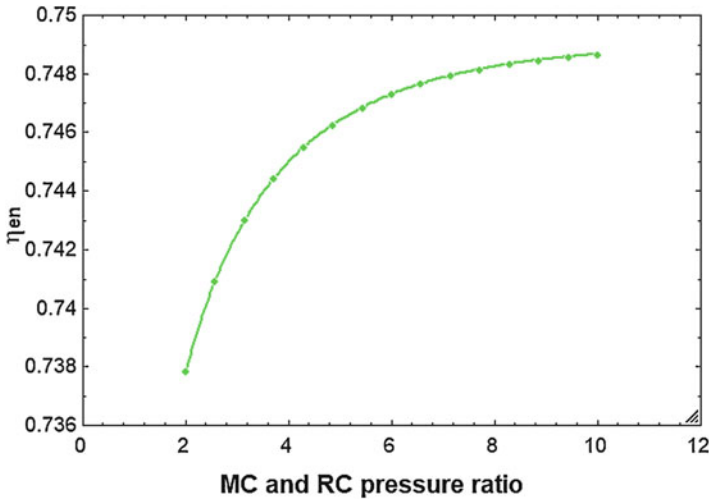


Fig. 5.6 Effect of MC and RC pressure ratio on thermal efficiency of the system

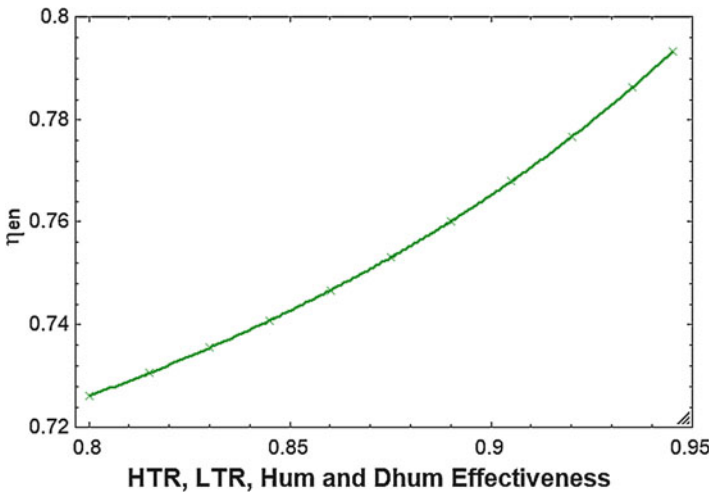
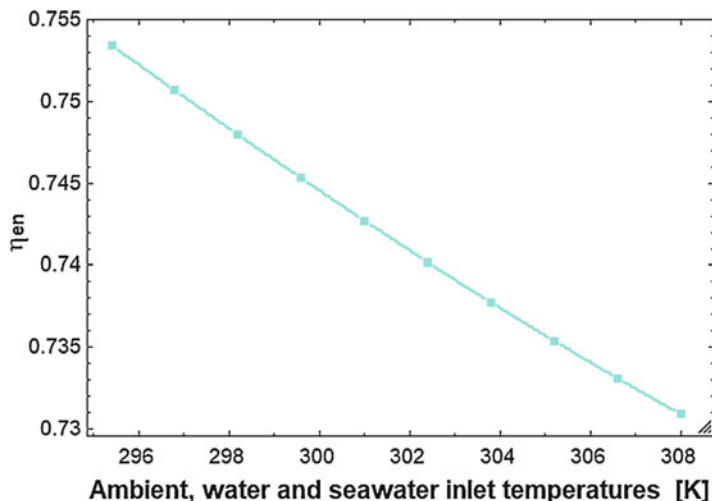


Fig. 5.7 Effect of HTR, LTR, Hum, and Dhum effectiveness on thermal efficiency of the system

### 5.5.6 Effect of Ambient, Water, and Seawater Inlet Temperatures

According to Fig. 5.8, ambient temperature is one of the most important parameters that plays a significant role in energy efficiency. Also, the ambient temperature is the same value of DHW and HU inlet water temperatures and seawater inlet temperature



**Fig. 5.8** Effect of ambient, water, and seawater inlet temperatures on thermal efficiency of the system

to the HDH system. When ambient temperature increases, net power, DHW, and desalination heat transfer rates decrease more than the increase in heating and cooling values. So, the overall energy efficiency will be decreased and it is good idea to use proposed system in cold regions to maximize the first law efficiency.

### 5.5.7 Effect of T-CO<sub>2</sub> Compressor to Turbine Electricity Ratio

Power consumption of T-CO<sub>2</sub> compressor is one of the most important parameters that affects energy efficiency. With increasing electricity ratio, solar, heating, and DHW energies are constant, but net power output will be decreased slowly and cooling and desalination products will be increased rapidly. So, conforming to Fig. 5.9, the enhancement of electricity ratio causes the growth of energy efficiency and it is appropriate option to raise T-CO<sub>2</sub> power consumption.

## 5.6 Concluding Comments

An innovative MGS integrated with a STP plant was devised in this chapter to produce cooling, power, freshwater, heating, and hot water simultaneously. For this aim, a S-CO<sub>2</sub> power cycle, a T-CO<sub>2</sub> refrigeration cycle, and a HDH unit were used in a more efficient configuration. The results of simulation indicated a promising outcome of the proposed arrangement. It was found that the devised multi-

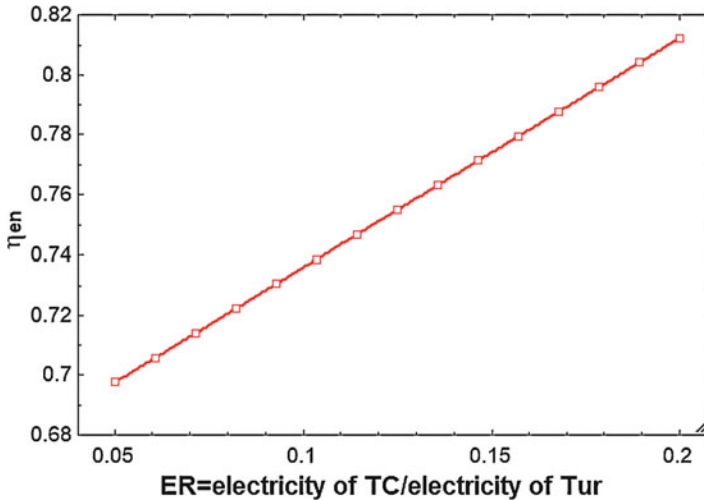


**Fig. 5.9** Effect of T-CO<sub>2</sub> compressor to turbine electricity ratio on thermal efficiency of the system

generation system has energy efficiency of 74.81% and can produce net electricity of 1335 kW, desalinated water of 34.79 m<sup>3</sup>/day, refrigeration load of 200 kW, heating load of 2870 kW, and hot water of 633 kW. Under such design circumstance, it was discerned that the energy efficiency can further be increased by increasing the receiver concentration ratio, compressor ratios, effectiveness of heat exchangers, and supplying more power from the power cycle to the mechanical T-CO<sub>2</sub>-driven refrigeration cycle or by decreasing ambient temperature, generator pinch point temperature, and direct normal irradiance.

## References

1. Dincer, I., & Rosen, M. A. (2012). *Exergy: Energy, environment and sustainable development*. Newnes. London: Elsevier
2. Kalogirou, S. A. (2013). *Solar energy engineering: Processes and systems*. Burlington: Academic.
3. Yilmaz, F. (2018). Thermodynamic performance evaluation of a novel solar energy based multigeneration system. *Applied Thermal Engineering*, 143, 429–437.
4. Yuksel, Y. E., Ozturk, M., & Dincer, I. (2019). Energetic and exergetic assessments of a novel solar power tower based multigeneration system with hydrogen production and liquefaction. *International Journal of Hydrogen Energy*, 44(26), 13071–13084.
5. Yilmaz, F., Ozturk, M., & Selbas, R. (2020). Development and performance analysis of a new solar tower and high temperature steam electrolyzer hybrid integrated plant. *International Journal of Hydrogen Energy*, 45, 5668.
6. Wu, H., et al. (2019). Performance investigation of a novel multi-functional system for power, heating and hydrogen with solar energy and biomass. *Energy Conversion and Management*, 196, 768–778.

7. El-Emam, R. S., & Dincer, I. (2018). Development and assessment of a novel solar heliostat-based multigeneration system. *International Journal of Hydrogen Energy*, *43*(5), 2610–2620.
8. Narayan, G. P., et al. (2010). Thermodynamic analysis of humidification dehumidification desalination cycles. *Desalination and Water Treatment*, *16*(1–3), 339–353.
9. Jamel, M., Abd Rahman, A., & Shamsuddin, A. (2013). Performance evaluation of molten salt cavity tubular solar central receiver for future integration with existing power plants in Iraq. *Australian Journal of Basic and Applied Sciences*, *7*(8), 399–410.
10. Li, X., et al. (2010). Thermal model and thermodynamic performance of molten salt cavity receiver. *Renewable Energy*, *35*(5), 981–988.
11. Xu, C., et al. (2011). Energy and exergy analysis of solar power tower plants. *Applied Thermal Engineering*, *31*(17–18), 3904–3913.
12. Narayan, G. P., McGovern, R. K., & Zubair, S. M. (2012). High-temperature-steam-driven, varied-pressure, humidification-dehumidification system coupled with reverse osmosis for energy-efficient seawater desalination. *Energy*, *37*(1), 482–493.
13. Narayan, G. P., John, M. G. S., & Zubair, S. M. (2013). Thermal design of the humidification dehumidification desalination system: An experimental investigation. *International Journal of Heat and Mass Transfer*, *58*(1–2), 740–748.
14. Farsi, A., Ameri, M., & Mohammadi, S. (2018). Application of transcritical CO<sub>2</sub> in multi-effect desalination system: Energetic and exergetic assessment and performance optimization. *Desalination and Water Treatment*, *135*, 108–123.
15. Mohammadi, Z., Fallah, M., & Mahmoudi, S. S. (2019). Advanced exergy analysis of recompression supercritical CO<sub>2</sub> cycle. *Energy*, *178*, 631–643.
16. Ma, Y., et al. (2019). Optimal integration of recompression supercritical CO<sub>2</sub> Brayton cycle with main compression intercooling in solar power tower system based on exergoeconomic approach. *Applied Energy*, *242*, 1134–1154.
17. Dincer, I., Midilli, A., & Kucuk, H. (2014). *Progress in exergy, energy, and the environment*. Cham: Springer.
18. Sachdeva, J., & Singh, O. (2019). Thermodynamic analysis of solar powered triple combined Brayton, Rankine and organic Rankine cycle for carbon free power. *Renewable Energy*, *139*, 765–780.
19. Parikhani, T., et al. (2020). Thermodynamic and thermoeconomic analysis of a novel ammonia-water mixture combined cooling, heating, and power (CCHP) cycle. *Renewable Energy*, *145*, 1158–1175.
20. Ahmadi, P., Dincer, I., & Rosen, M. A. (2013). Thermodynamic modeling and multi-objective evolutionary-based optimization of a new multigeneration energy system. *Energy Conversion and Management*, *76*, 282–300.
21. Pérez-García, V., et al. (2016). Comparative analysis of energy improvements in single transcritical cycle in refrigeration mode. *Applied Thermal Engineering*, *99*, 866–872.
22. Rostamzadeh, H., et al. (2018). Performance assessment and optimization of a humidification dehumidification (HDH) system driven by absorption-compression heat pump cycle. *Desalination*, *447*, 84–101.